Mechanochemical Activation of Covalent Bonds in Polymers with Full and Repeatable Macroscopic Shape Recovery

Supporting Information

Gregory R. Gossweiler,[†] Gihan B. Hewage,[†] Gerardo Soriano,[†] Qiming Wang,[‡] Garrett W. Welshofer,[†] Xuanhe Zhao,[‡] Stephen L. Craig*[†]

[†]*Department of Chemistry, Duke University, Durham, North Carolina 27708*

[‡]*Department of Mechanical Engineering and Materials Science, Duke University, Durham, North Carolina 27708*

**To whom correspondence should be addressed:*

Phone: (919) 660-1538. Fax: (919) 660-1605. Email: stephen.craig@duke.edu

Table of Contents

I. General Procedures

a. General Information. Dry solvents were obtained from Sigma-Aldrich and purified with a PureSolv™ solvent purification system before use. $CDCl_3$ and DMSO-d_6 were purchased from Cambridge Isotope Laboratories. All other reagents were purchased from Sigma-Aldrich® or Alfa Aesar® and used without further purification. Sylgard® 184 was purchased from Ellsworth Adhesives, Germantown, WI. All solvent used to solvent cast PDMS was passed through a plug of activated basic alumina (58 Å pore, ~150 mesh) before use. The inhibitor was removed from chloroform by stirring a 10:1 mixture of chloroform and concentrated sulfuric acid for 6 hours, washing extensively with water until neutral, and distilling under reduced pressure. As a caution, the chloroform must not be stored as the primary byproduct of degradation is phosgene. All glassware was dried overnight in an oven (160 °C) cooled under an inert gas. All reactions were performed under nitrogen, and anthracene reactions were protected from light wherever possible to minimize photochemical side-reactions. Thin layer chromatography was conducted on glass-backed Silicycle Siliaplate™ hard layer TLC plates (60 Å particle size, 250 μm, F-254 indicator). Column chromatography was performed using Silicycle SiliaFlash® F60 gel (40-63 μm particle size, 230-400 mesh).

b. Characterization. NMR spectra (^{1}H and ^{13}C) were obtained on either a 400 MHz Varian INOVA or 500 MHz Varian UNITY spectrophotometer. Chemical shifts are recorded as parts per million (ppm) referenced to the residual ^{1}H or ^{13}C peak at 7.26 ppm in $CDCl_3$ or 2.50 ppm in DMSO-d_6, or 77.16 ppm in $CDCl_3$ and 39.52 ppm in DMSO-d_6, respectively. ^{1}H shifts are reported as chemical shift, multiplicity, coupling constant if applicable, and relative integral. ^{1}H multiplicity reported as: s (singlet), d (doublet), dd (doublet of doublets), dt (doublet of triplets), ddd (doublet of doublet of doublets), ddt (doublet of doublet of triplets) t (triplet), td (triplet of doublets), q (quartet), mp (multiplet), or b (broad). Coupling constants (J) are reported in Hertz. High-resolution mass spectrometry was performed on an Agilent LCMS-TOF–DART at Duke University's Mass Spectrometry Facility.

c. Mechanical Testing. Uniaxial tensile tests were performed on a TA Instruments RSA III Dynamic Mechanical Analyzer (Force resolution: 0.0001 N, strain resolution: 1 nm) at Duke University's Shared Material Instrument Facility (SMIF). An environmental control chamber allows testing at room temperature up to 600 °C (reported heating rate of 0.1 to 60°C/min). For tensile tests we experienced issues with slipping at high strains. For this reason, additional pieces of 1:10 Sylgard® 184 (0.3 - 0.4 mm thick) were placed on each side of the sample film within the clamps of test fixture tool. The PDMS sandwich structure provided increased friction and prevented slipping at high strains.

d. Fluorescence Microscopy. Fluorescent images were obtained on a Zeiss Axio Observer A1 inverted microscope outfitted with a Zeiss HBO arc lamp and power supply. Images were acquired on a Hamamatsu Orca ER digital monochrome camera using the MetaMorph® 7.7.3 platform and saved as 16-bit TIFF images. The objective used was a 5x/0.16 Ph1 440321-9902: EC Plan-Neofluar, NA: 0.16, air, Ph1, WD: 18.5 mm. Reported width of a pixel is 1.2623 μm. Fluorescent filter chosen for the anthracene study was a DAPI cube (FS49: G365, FT395, BP445/50).

e. Spectroscopy. Steady state emission spectra were recorded on an Edinburgh Instruments FLSP 920 spectrofluorimeter equipped with a 450 W xenon lamp as the excitation source and a Hamamatsu R2658 PMT detector. Visible absorption spectra were obtained on a Varian Cary 500 UV-Vis Spectrophotometer. Films were uniaxially elongated perpendicular (excitation) or oriented 45°

(emission) to the beam path via a customized Velmex Left-Right Screw Motion UniSlide® (Catalog Number: A1512C-S1.5-LR).

f. Digital Photography. All images were captured on a Canon EOS RebelTM xsi with a Canon EF-S 18-55 mm f/3.5-5.6 IS SLR lens. Images were obtained under ambient room lighting without flash with general exposure settings of 1/50 sec, *f*/4.8, ISO 400. Images were captured in .CR2 raw format to prevent an automatic color correction from the digital camera, maintaining the trueness of the data in case we wanted to analyze the individual RGB pixel intensities. All images required post-processing and were captured with a color-neutral target (Opteka™ Digital Color & White Balance Card) in the background to facilitate white balancing and standardization. Raw images available upon request.

II. Synthetic Procedures

a. Synthetic Schemes

iv. Active Spiropyran

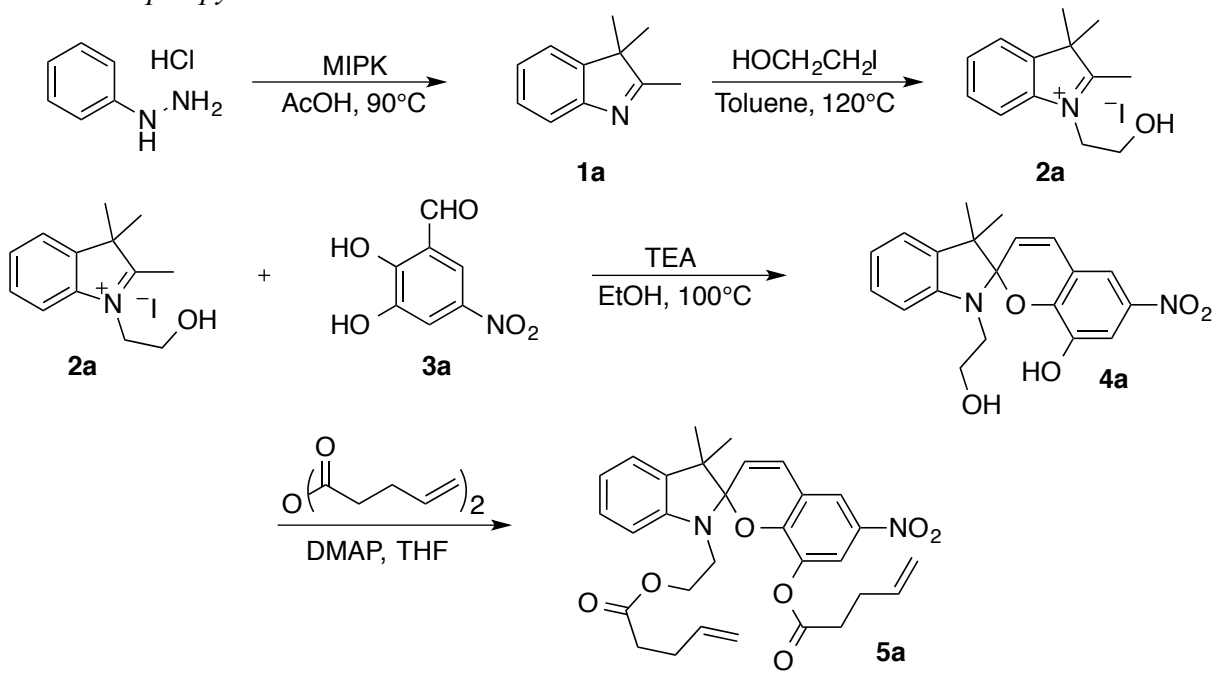

v. Control Spiropyran

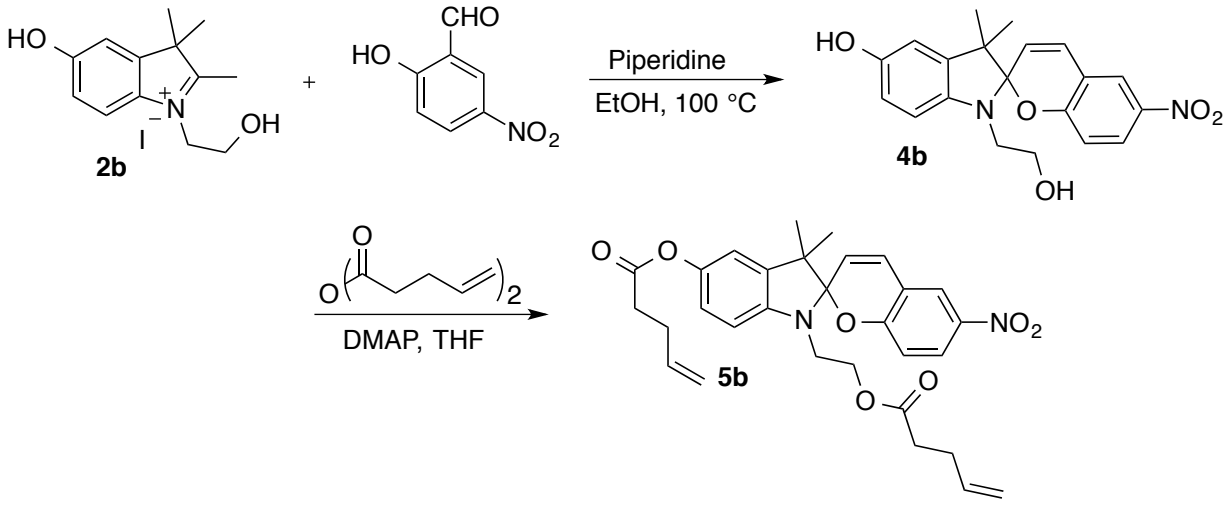

vi. Functional Anthracene

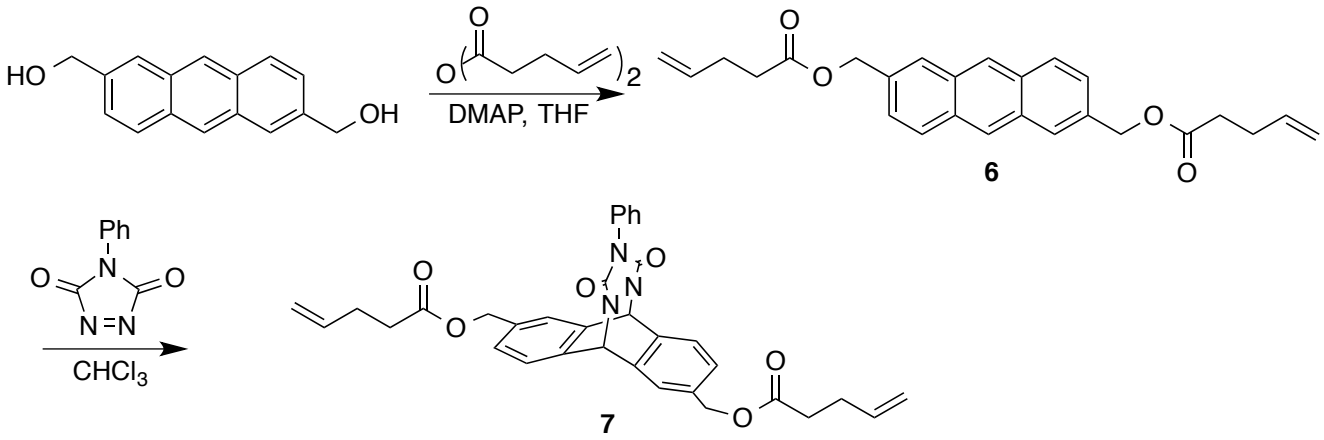

b. Small Molecule Synthesis

iv. Active Spiropyran

Compound (**1a)**: *2,3,3-trimethyl-3H-indole*

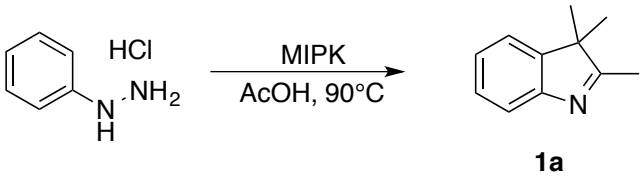

A solution of phenylhydrazine hydrochloride (15.0 g, 103 mmol, 1.0 equiv) and 3-methyl-2-butanone (MIPK) (13.3 mL, 124 mmol, 1.2 equiv) in 300 mL AcOH was heated to 90°C. After 8 hr. solvents

were removed *in vacuo* to yield a dark red oily solid. To this solid was added 100 mL H_2O and the solution was basified to *ca.* pH 10-11 with 40 mL of a 2M NaOH solution. The product was extracted with Et_2O (3 x 100 mL), dried with Mg_2SO_4, and concentrated *in vacuo* to yield a viscous red oil. The oil was purified by vacuum distillation (60°C, < 100 mTorr) to yield **1a** as a light yellow oil, which turned to a yellow solid upon freezing (14.5 g, 91.1 mmol, 87.6%).

^{1}H NMR (400 MHz, $CDCl_3$) δ 7.52 (d, *J* = 7.6 Hz, 1H), 7.33 – 7.23 (m, 2H), 7.18 (td, *J* = 7.4, 0.9 Hz, 1H), 2.27 (s, 3H), 1.29 (s, 6H).
^{13}C NMR (126 MHz, $CDCl_3$) δ 187.14, 153.26, 145.12, 127.01, 124.56, 120.75, 119.32, 52.98, 22.51, 14.82.
HRMS-ESI (m/z): $[M + H]^+$ calcd for $C_{11}H_{13}N$, 160.1221; found, 160.1223.

Compound (**2a**): *2-hydroxyethyl-2,3,3-trimethyl-3H-indolium iodide*

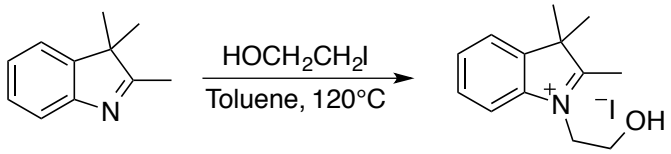

1a **2a**

A solution of **1a** (10.0 g, 62.8 mmol, 1.0 equiv) and 2-iodoethanol (7.34 mL, 94.2 mmol, 1.2 equiv) in 105 mL dry toluene was heated to reflux. After 18 hr. the suspension was cooled to 0°C and the solid was collected by vacuum filtration. Solids were washed with 100 mL of a 2% (v/v) solution of EtOH in Et_2O and was dried under high vacuum overnight to yield **2a** as a light yellow solid (19.4 g, 58.7 mmol, 93.5%).

^{1}H NMR (400 MHz, DMSO-*d*6) δ 8.01 – 7.93 (m, 1H), 7.89 – 7.83 (m, 1H) , 7.69 – 7.58 (m, 2H), 4.66 – 4.55 (m, 2H), 3.94 – 3.83 (m, 2H), 2.82 (s, 3H), 1.55 (s, 6H).
^{13}C NMR (126 MHz, DMSO-*d*6) δ 197.74, 141.81, 141.11, 129.32, 128.82, 123.52, 115.61, 57.81, 54.29, 50.34, 22.04, 14.59.
HRMS-ESI (*m/z*): $[M + H - I]^+$ calcd for $C_{13}H_{18}INO$, 204.1383; found, 204.1384.

Compound (**3a**): *2,3-dihydroxy-5-nitrobenzaldehyde*

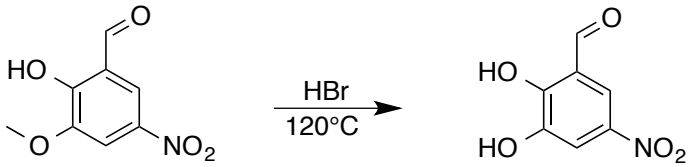

3a

3a was synthesized as previously reported,[1] with modification to the work up. The combined organic fractions and precipitate were dissolved in DCM, stirred with activated carbon for 30 min and passed through a plug of celite. The solid was then recrystallized from boiling EtOAc. Characterization matched literature reported values.

^{1}H NMR (400 MHz, $CDCl_3$) δ 11.76 (s, 1H), 9.99 (s, 1H), 8.19 (d, *J* = 2.6 Hz, 1H), 8.05 (d, *J* = 2.5 Hz, 1H), 5.94 (s, 1H).
^{1}H NMR (500 MHz, DMSO-d_6) δ 11.12 (br, 2H), 10.24 (s, 1H), 7.90 (s, 1H), 7.70 (s, 1H).

^{13}C NMR (126 MHz, DMSO-d_6) δ 189.77, 156.16, 147.27, 139.19, 121.79, 114.61, 113.14.

Compound (**4a**): *1'-(2-hydroxyethyl)-3',3'-dimethyl-6-nitrospiro[chromene-2,2'-indolin]-8-ol*

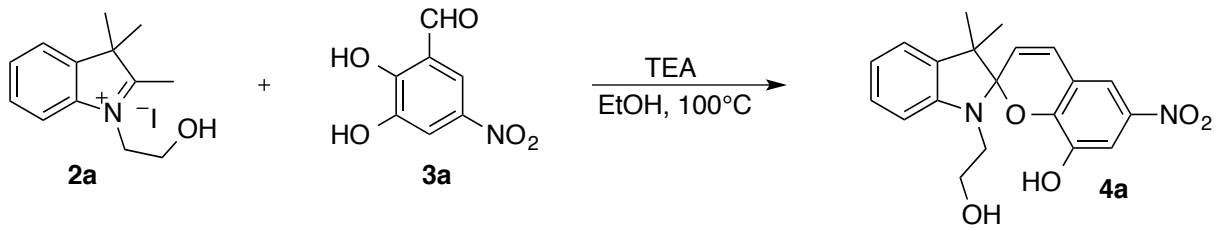

To a solution of **2a** (5.17 g, 15.6 mmol, 1.0 equiv) and **3a** (2.86 g, 15.6 mmol, 1.0 equiv) in 150 mL EtOH (absolute) was added triethylamine (4.37 mL, 31.2 mmol, 2 equiv). The solution was brought to reflux and was stirred for 2 hr. The solution was then cooled, filtered, and the precipitate washed with cooled ethanol to yield **4a** as a dark green solid (on some attempts the solid failed to precipitate, concentrated the solution to half its original volume allowed the solid to crash out) (3.84 g, 10.4 mmol, 66.7%).

^{1}H NMR (500 MHz, DMSO-*d*6, HCl) δ 8.52 (d, *J* = 2.5 Hz, 1H), 8.50 (d, *J* = 16.6 Hz, 1H), 8.06 – 7.95 (m, 2H), 7.95 – 7.82 (m, 2H), 7.65 – 7.55 (m, 2H), 4.82 (b, 2H), 4.04 – 3.74 (m, 2H), 1.79 (s, 6H).
^{13}C NMR (126 MHz, DMSO-*d*6, HCl) δ 183.44, 153.70, 146.78, 146.43, 143.94, 141.17, 139.97, 129.68, 129.18, 123.16, 121.14, 116.05, 115.97, 115.24, 112.60, 58.67, 52.61, 49.96, 26.42.
HRMS-ESI (m/z): $[M + H]^+$ calcd for $C_{20}H_{20}N_2O_5$, 369.1445; found, 369.1456.

Compound (**5a**): *3',3'-dimethyl-6-nitro-1'-(2-(pent-4-enoyloxy)ethyl)spiro[chromene-2,2'-indolin]-8-yl pent-4-enoate*

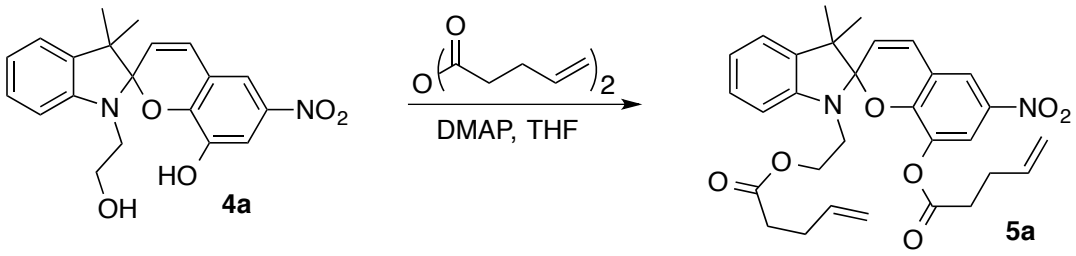

To compound **4a** (0.20 g, 0.54 mmol, 1.0 equiv) and 4-dimethylaminopyridine (DMAP) (0.12 g 0.97 mmol, 1.8 equiv) in 5 mL THF was added 4-pentenoic anhydride (0.26 mL, 1.4 mmol, 2.6 equiv). After stirring for 3 hr. the reaction was quenched with MeOH (0.5 mL) and was stirred for an additional 10 min. The crude reaction mixture was passed through a plug of basic alumina and eluted from the column with DCM. Concentration of the solution *in vacuo* yielded a viscous purple oil, which was dried overnight under high vacuum and subsequently recrystallized from boiling hexane to yield **5a** as a yellow solid (0.26 g, 0.49 mmol, 90%).

^{1}H NMR (400 MHz, $CDCl_3$) δ 7.95 (d, *J* = 2.6 Hz, 1H), 7.82 (d, *J* = 2.6 Hz, 1H) , 7.16 (td, *J* = 7.7, 1.2 Hz, 1H) , 7.10 – 7.03 (m, 1H) , 6.96 (d, *J* = 10.5 Hz, 1H) , 6.91 – 6.82 (m, 1H) , 6.66 (d, *J* = 7.8 Hz, 1H) , 5.96 (d, *J* = 10.4 Hz, 1H) , 5.84 – 5.70 (m, 1H) , 5.55 (ddt, *J* = 16.9, 10.7, 6.3 Hz, 1H) , 5.05 – 4.85 (m, 4H), 4.31 – 4.09 (m, 2H), 3.33 (t, *J* = 6.4 Hz, 2H), 2.46 – 2.26 (m, 4H), 2.26 – 2.08 (m, 2H), 1.91 – 1.80 (m, 2H), 1.27 (s, 3H), 1.18 (s, 3H).

^{13}C NMR (126 MHz, $CDCl_3$) δ 172.94, 170.48, 150.91, 146.65, 140.33, 137.75, 136.62, 136.36, 135.85, 128.46, 127.89, 121.69, 121.55, 120.32, 120.19, 119.32, 119.29, 115.73, 115.54, 107.51, 107.14, 62.63, 52.33, 42.56, 33.54, 32.96, 28.83, 28.44, 25.98, 19.48.
HRMS-ESI (*m/z*): $[M + H]^+$ calcd for $C_{30}H_{32}N_2O_7$, 533.2282; found, 533.2293.

v. Control Spiropyran

Compound (**5b**): 1'-(2-hydroxyethyl)-3', 3'-dimethyl-6-nitrospiro[chromene-2,2'-indolin]-5'-ol

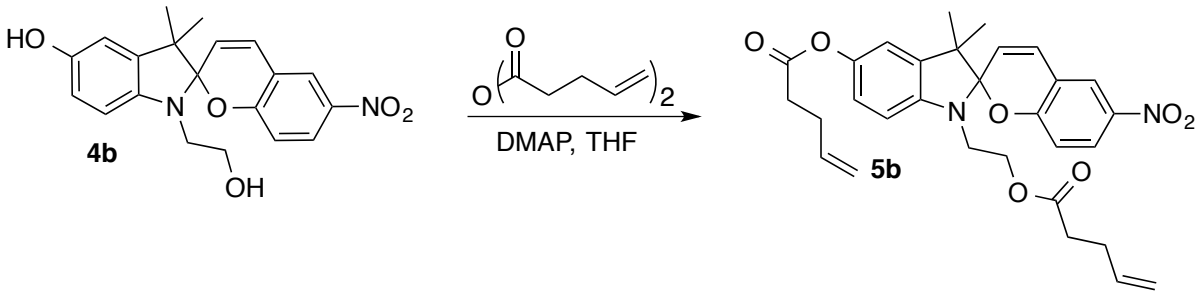

To compound **4b**[1] (0.25 g, 0.68 mmol, 1.0 equiv) and 4-dimethylaminopyridine (DMAP) (0.12 g 0.97 mmol, 0.15 g, 1.2 mmol, 1.8 equiv.) in 5 mL THF was added 4-pentenoic anhydride (0.34 mL, 1.8 mmol, 2.6 equiv.). After stirring for 3 hr. the reaction was quenched with MeOH (0.5 mL) and was stirred for an additional 10 min. At which point the reaction mixture was passed through a plug of basic alumina and eluted from the column with DCM. Concentrating the eluent *in vacuo* yielded pure **5b** as a viscous yellow oil (0.22 g, 0.41 mmol, 60%).

^{1}H NMR (400 MHz, $CDCl_3$) δ 8.04 (ddd, *J* = 8.9, 2.7, 0.8 Hz, 1H) , 8.01 (d, *J* = 2.6 Hz, 1H) , 7.34 – 7.11 (m, 1H) , 6.93 (d, *J* = 10.4 Hz, 1H) , 6.89 (ddd, *J* = 8.3, 2.3, 0.9 Hz, 1H) , 6.82 (d, *J* = 2.3 Hz, 1H) , 6.78 (d, *J* = 8.8 Hz, 1H) , 6.65 (d, *J* = 8.4 Hz, 1H) , 5.88 (d, *J* = 10.2 Hz, 1H) , 6.00 – 5.70 (m, 3H), 5.24 – 4.93 (m, 4H), 4.22 (ddt, *J* = 30.5, 11.8, 6.3 Hz, 2H), 3.43 (ddt, *J* = 44.8, 15.0, 6.3 Hz, 2H), 2.67 (t, *J* = 7.4 Hz, 2H), 2.53 (q, *J* = 7.2 Hz, 2H), 2.41 – 2.30 (m, 4H), 1.26 (s, 3H), 1.18 (s, 3H).
^{13}C NMR (126 MHz, cdcl3) δ 172.53, 171.89, 158.98, 144.15, 144.03, 140.91, 136.57, 136.16, 128.17, 125.79, 122.53, 121.22, 120.03, 118.07, 115.61, 115.52, 115.38, 115.32, 106.45, 62.09, 52.59, 42.31, 33.38, 33.11, 28.69, 28.44, 25.49, 19.52.
HRMS-ESI (*m/z*): $[M + H]^+$ calcd for $C_{30}H_{32}N_2O_7$, 533.2282; found, 533.2277.

vi. Functional Anthracene

*Compound (***6***): anthracene-2,6-diylbis(methylene) bis(pent-4-enoate)*

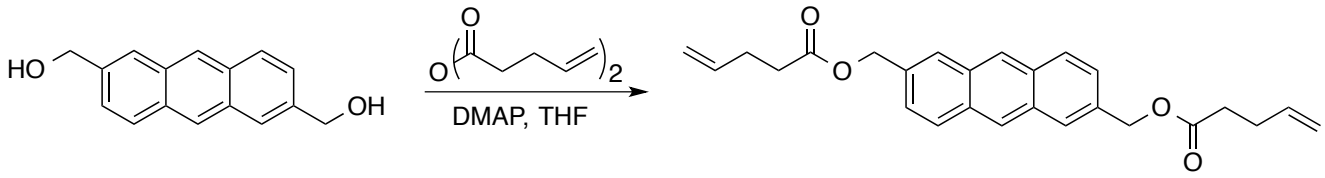

Anthracene-2,6-dimethanol was made as previously reported (Characterization matched literature reported values, ^{13}C spectrum attached).[2-4] To a slurry of 2,6-anthracenemethanol (73 mg, 0.31 mmol, 1.0 equiv) in 8 mL dry THF was added 4-dimethylaminopyridine (DMAP) (0.11 g 0.92 mmol, 3.0 equiv). The solution was cooled to 0 °C and pentenoic anhydride (0.15 mL, 0.80 mmol, 2.6 equiv) was

added dropwise and the solution was allowed to warm to RT. After 2 hours, 5 mL MeOH was added, and the solution was stirred for 15 minutes and concentrated *in vacuo*. The crude solid was taken up in 100 mL DCM, washed with (2 x 50 mL) 1% HCl followed by (2 x 50 mL) H_2O. The organic layer was dried over Na_2SO_4 and concentrated. The resulting solid was purified by silica gel chromatography (20% EtOAc:Hex, r.f. = 0.6) and recrystallized from absolute EtOH to yield **6** as a yellow solid (93 mg, 0.23 mmol, 75%).

^{1}H NMR (400 MHz, $CDCl_3$) δ 8.41 (s, 1H) , 8.01 (d, *J* = 8.7 Hz, 1H) , 7.96 (s, 1H) , 7.44 (dd, *J* = 8.7, 1.6 Hz, 1H) , 5.85 (ddt, *J* = 16.6, 10.1, 6.2 Hz, 1H) , 5.32 (s, 2H), 5.14 – 4.98 (m, 2H), 2.58 – 2.49 (m, 2H), 2.49 – 2.39 (m, 2H).
^{13}C NMR (126 MHz, $CDCl_3$) δ 173.09, 136.69, 133.16, 131.54, 128.90, 127.47, 126.52, 125.76, 115.78, 77.40, 77.15, 76.90, 66.57, 33.69, 29.01.
HRMS-ESI (*m/z*): $[M + H]^+$ calcd for $C_{26}H_{26}O_4$, 403.2632; found, 403.2631.

*Compound (***7***): Anthracene Adduct*

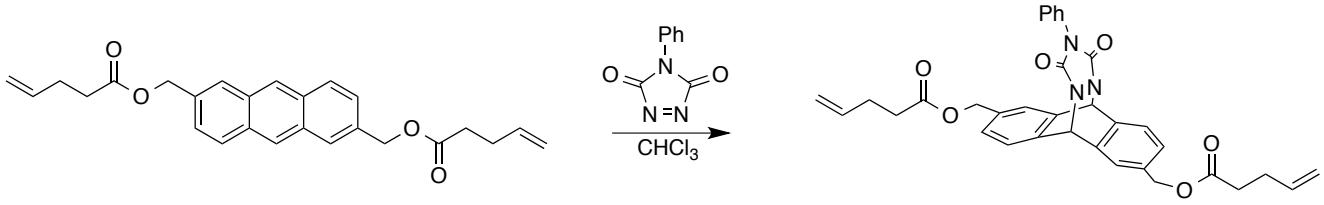

To a flame-dried flask was added anthracene-2,6-diylbis(methylene) bis(pent-4-enoate) (0.050 g, 0.124 mmol, 1 eq.), 4-phenyl-1,2,4-triazoline-3,5-dione (0.026 g, 0.148 mmol, 1.2 eq.), and 4 mL dry chloroform. The solution was stirred for 1.5 hrs at r.t. and was concentrated in vacuo. The resulting solid was purified by silica gel chromatography (20% EtOAc:Hex, r.f. = 0.2) to yield **7** (0.062 g, 0.104 mmol, 84%).

^{1}H NMR (400 MHz, $CDCl_3$) δ 7.48 (d, *J* = 7.2 Hz, 2H), 7.42 – 7.32 (m, 1H) , 7.32 – 7.25 (m, 2H), 7.25 – 7.18 (m, 1H) , 6.33 (s, 1H) , 5.80 (ddt, *J* = 16.3, 10.2, 6.2 Hz, 1H) , 5.11 (s, 2H), 5.08 – 4.94 (m, 2H), 2.50 – 2.42 (m, 2H), 2.42 – 2.32 (m, 2H).
^{13}C NMR (126 MHz, $CDCl_3$) δ 172.78, 155.96, 136.96, 136.78, 136.54, 136.37, 131.21, 129.16, 128.48, 128.25, 125.38, 124.43, 124.01, 115.79, 77.42, 77.17, 76.91, 65.59, 60.25, 33.55, 28.88.
HRMS-ESI (*m/z*): $[M + NH_4]^+$ calcd for $C_{34}H_{31}N_3O_6$, 595.2551; found, 595.2559

III. Active PDMS Film Preparation

a. General Information
Sylgard® 184 is a proprietary two-part (Base and Curing Agent, typically mixed in a 10:1 ratio) silicone elastomer comprising vinyl terminated poly(dimethylsiloxane), poly(methylhydrosiloxane-co-dimethylsiloxane) copolymer, amorphous silica, and a platinum catalyst. When the two components are mixed, a platinum catalyzed hydrosilylation reaction between the vinyl- and hydrosilane functionalities creates an intractable covalent network (Figure 1). Alkene functionalization of a molecule of interest allows for covalent incorporation by means of the hydrosilylation curing chemistry.

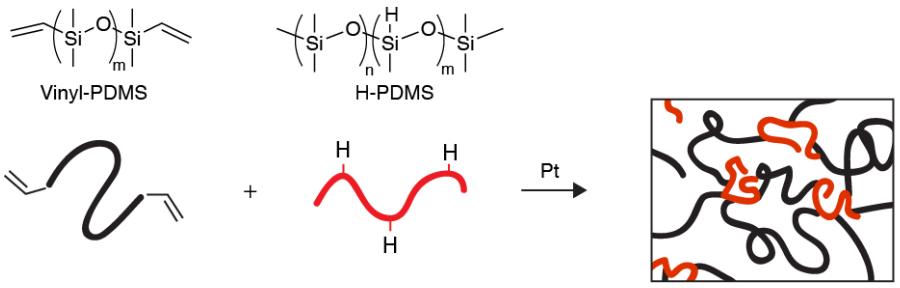

Figure 1. Blending vinyl terminated PDMS with a hydrosilane copolymer allows for a platinum catalyzed hydrosilylation to create a covalently cross-linked network.

b. Typical Procedure for Active Film Preparation

Sylgard® 184 Base (2.0 g) was added to a 20 mL scintillation vial followed by 0.2 mL of a 75 mg/mL solution of **5a** in xylenes. The solution was mixed to homogeneity with a vortex until the spiropyran was completely dispersed (pink cloudy coloration remains). To this mixture was added 0.2 g curing agent and the mixture was further mixed extensively with a vortex. The solution was then poured onto a PTFE surface (or biaxially-oriented poly(ethylene terephthalate) (BoPET), ultra-high-molecular-weight polyethylene (UHMWPE), polyoxymethylene (POM), polypropylene (PP), silicon wafer) and was cured in a vacuum oven at 65 °C for 16-24 hr. Once cured, the films can be easily pealed away and cut into strips for testing.

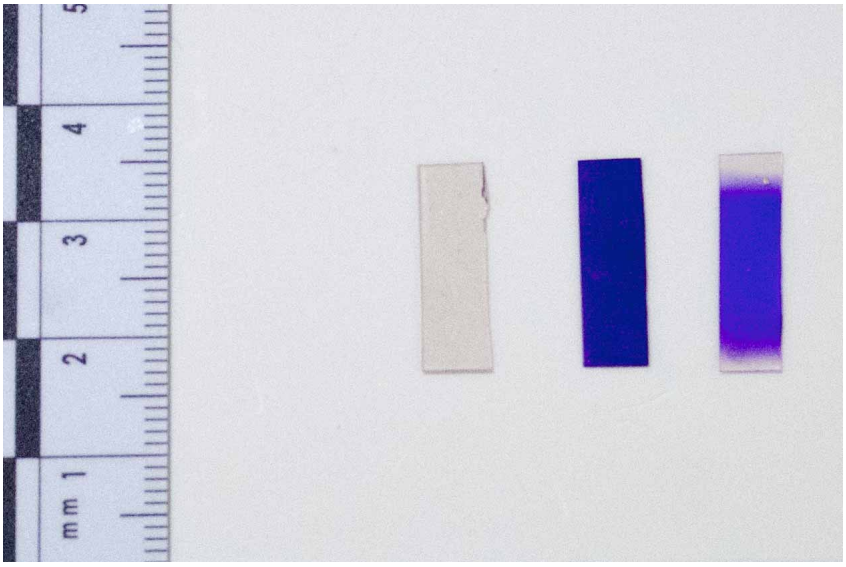

Figure 2. Active PDMS film strip cut from a larger sample (left), photochemically induced conversion to merocyanine (middle), tensile elongation sample showing mechanical activation (right).

Films are light yellow in color as compared to a virgin PDMS sample, presumably from spiropyran itself, which is not completely colorless. The cured sample against a true white background can be seen above (Figure 2, Left). Photochemically converting the incorporated spiropyran to merocyanine with 30 s illumination with an ultraviolet hand lamp (245 nm, 6 W) results in deep coloration of the sample (Figure 2, middle). Tensile elongation results in a color change within the gauge region of a hand-stretched sample (Figure 2, right). The thicknesses of the samples are 0.51, 0.46, and 0.40 mm from left to right.

IV. Mechanical Testing

a. Active Film Tensile Elongation

Tensile elongation of an active film results in the mechanical activation of spiropyran to merocyanine as the film is extended to high stretch ratios (Figure 3). Digital images of a film under tension can be used to determine the onset of mechanical activation by plotting the change in color intensities as a function of strain.

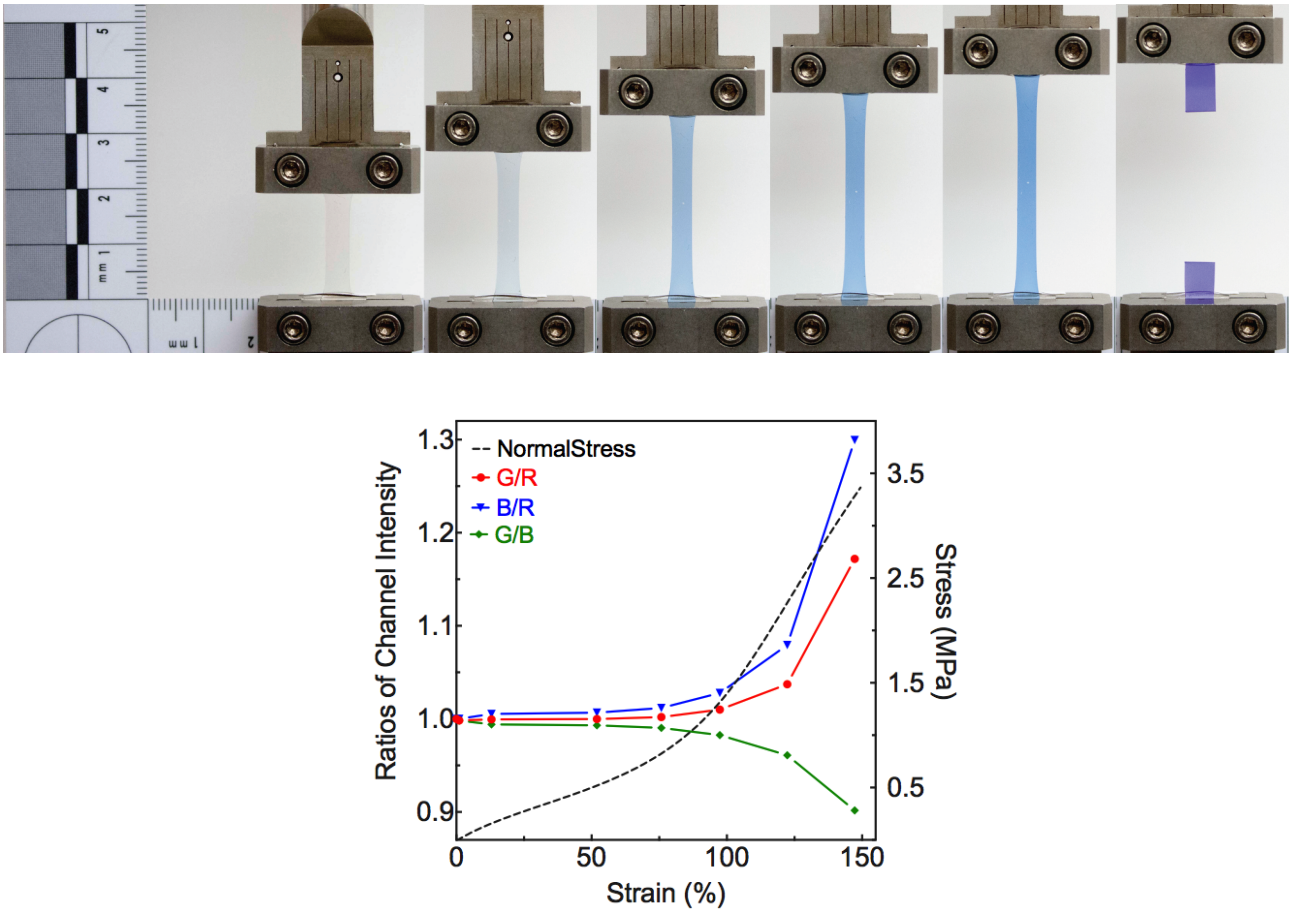

Figure 3. Tensile elongation of sample of active PDMS containing spiropyran (TOP) and a plot of the *ratio of RGB Color Channel Intensities (BOTTOM)*

Both the ratios of the Green/Red channels and the Blue/Red channels show a change in color between 75-100% strain, corresponding to the mechanical activation of spiropyran to merocyanine. The ratio of green to blue is shown to diminish as the active film is stretched further. A stress-strain curve within the same plot indicates that activation is greatest as the elastomer begins to strain harden (Figure 3).

b. Control Film Tensile Elongation

Films containing the control spiropyran were made in the same ratios as the active spiropyran films. Uniaxial elongation of the films shows no color change (Figure 4). When the film is well beyond the threshold strain for activation of SP to MC of an active film (i.e. >125%), the sample is illuminated with a 400 nm laser to photochemically convert the spiropyran to merocyanine in order to confirm the presence of the molecule. Pulling the film to failure reveals no color change (Figure 4).

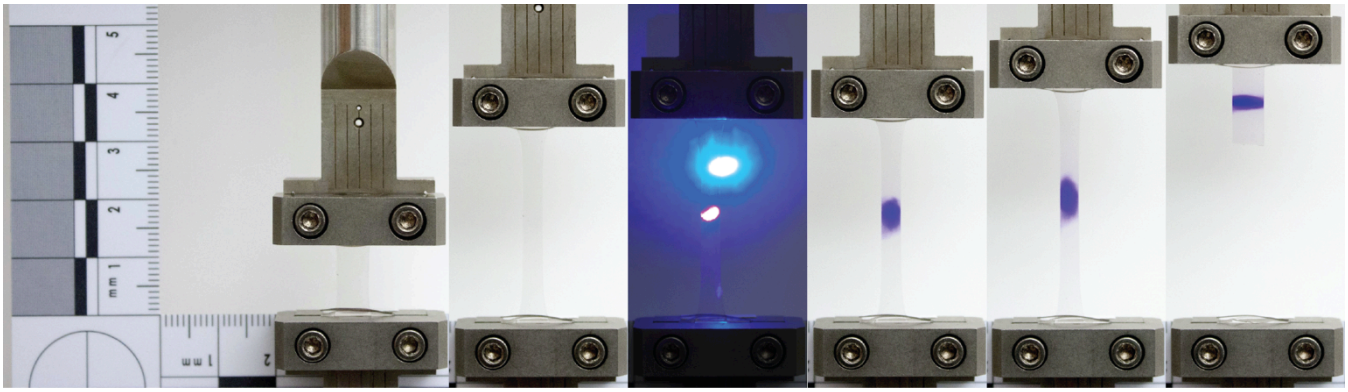

Figure 4. Stretching a film with containing a bis-funtional, mechanically insensitive control molecule (**5b**) does not result in a color change. Illuminating the sample with 400 nm light confirms the presence of the molecule.

b. Cyclic Activation

Demonstration of the reversible activation of spiropyran was conducted with the photochemical reversion of merocyanine to spiropyran with intense white light after each loading cycle. Shown are 10 cycles in which the material was strained to 175%, relaxed, illuminated to colorless, and again activated (Figure 5). From the images can be seen a gradual decrease in the peak color intensity as compared to the first cycle.

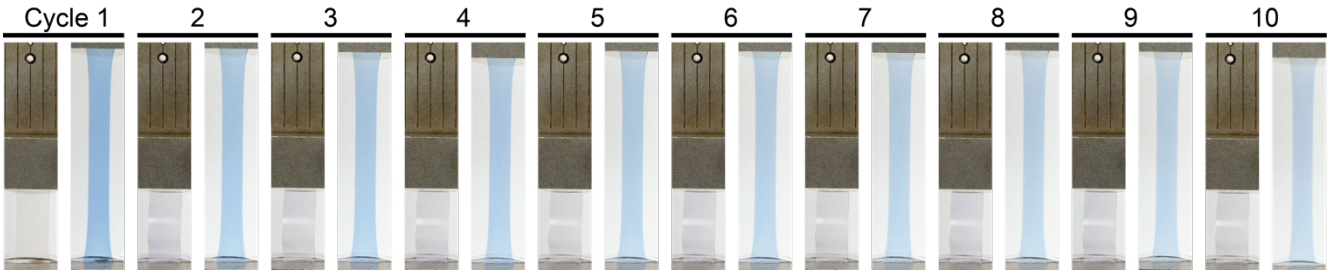

Figure 5. Ten cycles of reversible activation of the active PDMS test sample shows a gradual decrease in peak color intensity for increasing strains.

To assess whether the color was diminishing from a reduction in elastically reversible spiropyran chains (i.e. activation resulting from irrecoverable plastic loss prevents subsequent re-activation of the same spiropyran) we stretched film ten times in the dark, immediately captured an image, closed all merocyanine with bright white light, strained for an 11th time, and captured a subsequent image (Figure 6). It is reasonable to assume that if the mechanical activation of spiropyran to merocyanine were plastic in nature, and no light was present to close the "one-and-done" plastically activated merocyanine (timescale of thermal reversion to colorless is much larger than the experiment), then the image of the 10th cycle would be more intense in color than the first image. The 10th cycle shown here is nearly if not the same color intensity (Figure 6), at least to the naked eye.

Relaxing the sample and returning all open merocyanine to spiropyran, followed by a reloading of the film results in a color intensity that is indistinguishable from the first two (Figure 6). This result suggests that mechanochemical activation is elastic in nature in both from the macroscopic and molecular scale. The color loss shown in Figure 5 and in the manuscript is the result of another process that prevents the mechanical switching of spiropyran to merocyanine, presumably photooxidation.

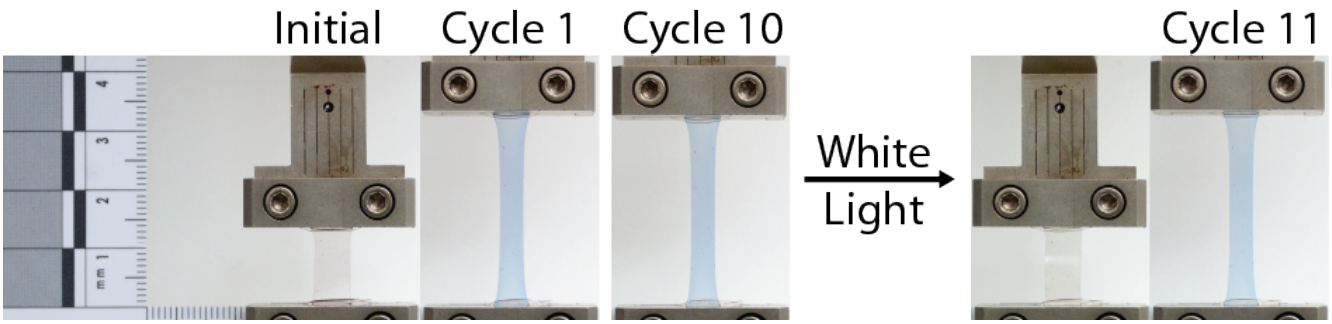

Figure 6 Ten cycles of stretching a film in in dark results in a sample color intensity that is nearly identical to the first cycle. Relaxing the sample, closing the merocyanine with white light, and stretching the sample results in a similarly colored film, suggesting that the same molecules of merocyanine activated on the first cycle are again activated on the 11th.

V. Elastomeric Sphere Compression and Analysis

a. Sphere Fabrication

Sylgard® 184 Base (36 g) was added to a 50 mL Eppendorf tube, followed by 4 mL of xylene containing 75 mg of **5a.** The mixture was blended extensively with a vortex to ensure complete mixing. To this mixture was added 3.6 g Curing Agent and the mixture further homogenized for an additional 3 minutes followed by 20 minutes of degassing under vacuum (*ca.* 10 Torr). The mold for the sphere was obtained by drilling a 1/4 inch hole in a standard 40 mm table tennis ball (inner volume approximately 33.5 mL). The table tennis ball was rinsed 3x with xylene and dried with compressed air. The degassed mixture was slowly added to the sphere by means of a syringe, taking care not to introduce any bubbles. After curing in an oven at 65°C for 24 hours the shell of the ball can be easily peeled away, leaving a cured sphere.

b. Compression of Active PDMS Sphere

The active spheres were manually compressed with a Carver laboratory press. The sample was oriented between two ¾" plastic blocks to protect the surface of the sphere and increase contrast. Upon compression the sphere sustains strains of over 50% before a noticeable color change can be observed (Figure 7), applying greater compressive stresses results in incrementally larger color changes.

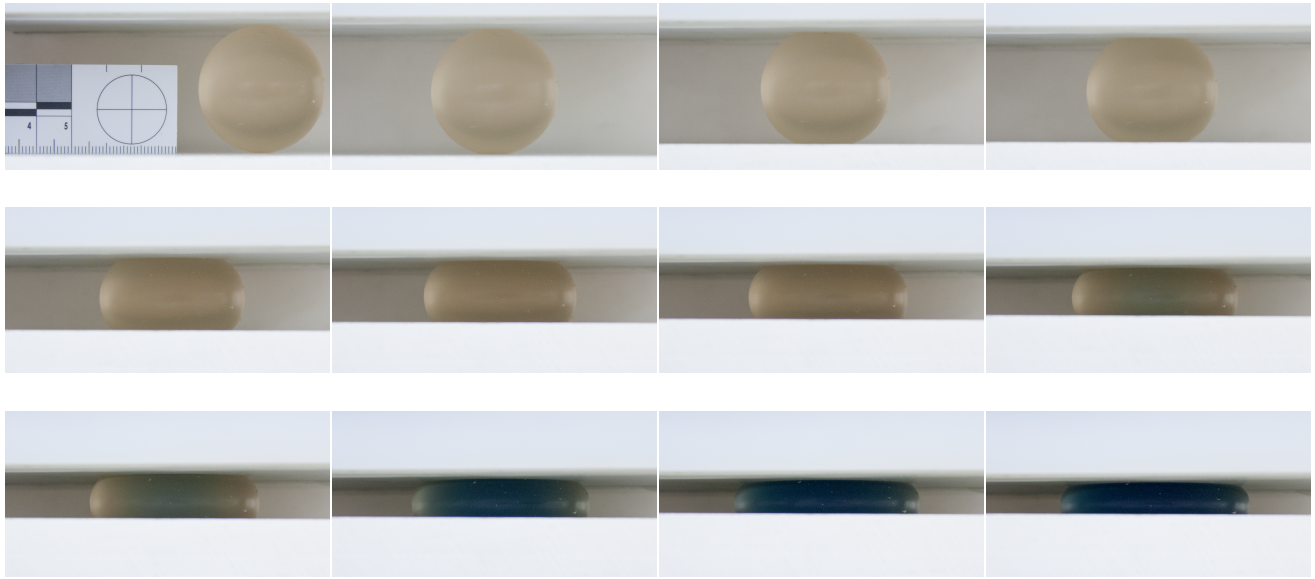

Figure 7. Compression of a 40 mm sphere leads to the mechanochemical activation of covalently bound spiropyran after *ca.* 60% strain. Removing the deformation allows the sphere to rebound, and the color to fade, which can then be reactivated on a subsequent compression.

Over 2 metric tons of force was required to compress the sphere to the maximum strain shown in the last image. Sphere compression is both reversible and repeatable, and the images shown here were obtained from a sphere that had been tested 2 days before. Interestingly, the sphere did not display the same blue to purple color shift upon relaxation as the uniaxial tension samples. Additionally, once the deformation was removed the blue color faded rapidly under ambient room light, returning to colorless in under 2 minutes. We speculate that some residual xylene may play a part in the different spiropyran switching behavior between sphere compression and film extension.

VI. Active PDMS Photoswitch Experiment

We sought to increase the stress within the network using the photochemical switching of stress-bearing merocyanine, as was shown previously.[5,6] Stress vs. time plots were obtained by elongating an active film sample to 125% strain and maintaining a static strain (Figure 8A). Illuminating the film sample with bright white light from a high power LED Maglite® (226 lumens, 4880 cd) results in increase in stress for the duration of illumination (100-150s, 250-300s, and 450-500s). However, when a comparably intense illumination source (3W LED array, SuperBrightLEDs: 8SMD-LED MR16 *warm white*, 3.2 lumen per LED, 260 lumen total) is shone on a sample treated under similar conditions (illumination from 90-120s, 180-210s, 270-300s), the curve does not display the same dramatic increase (Figure 8B). We discovered that the Maglite® put off enough heat to warm the sample. Instead of closing the merocyanine and increasing the measured stress, we speculate that we may instead have mistaken a fundamental characteristic of rubber elasticity for another phenomena; the heating of an elastic solid will cause it to contract. Repeating the MagLite® test with a 470 nm high pass filter (allowing the wavelengths of light that excite merocyanine to pass unimpeded, and insulating the sample from the light) resulted in no features in the curve (data not shown). Holding an open flame approximately 4-6 cm away resulted in sharp increases in the recorded stress (Figure 8C), followed by a cool down once the flame was removed.

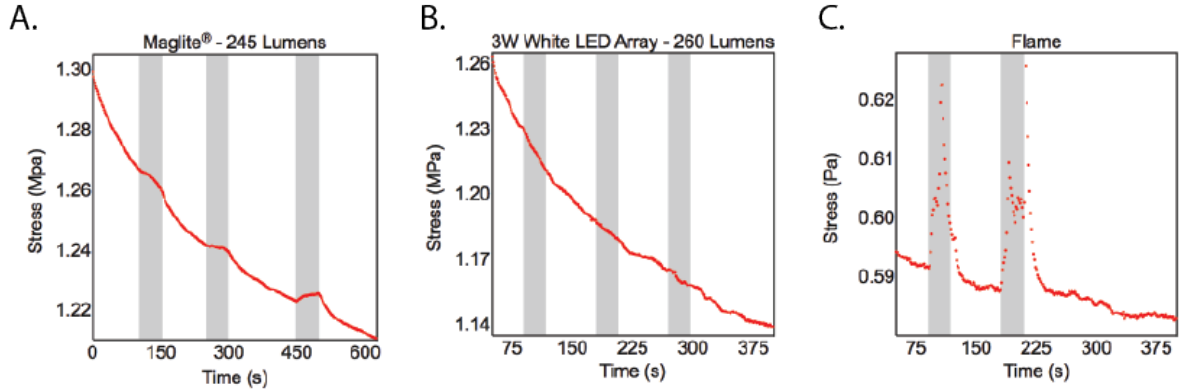

Figure 8. When a sample is stretched to 125% and illuminated with a bright LED flashlight there can be seen increases in stress corresponding to illumination time (**A**, gray region). However, when a second illumination source is chosen that is comparably intense, an LED array, the same trend is not observed (**B**). Straining a film and exposing it to an open flame approximately 4-6 cm in distance will cause sharp increases in stress, followed by a "cool-down" when the heat is removed (**C**).

VII. Anthracene retro-Diels-Alder Study

a. Active PDMS film preparation

Sylgard® 184 Base (4.5 g) was added to a 20 mL scintillation vial followed by 0.5 mL of a 40 mg/mL solution of **7** in dry, inhibitor free chloroform. The solution was mixed to homogeneity with a vortex until the compound was completely dispersed (cloudy white solution). To this mixture was then added

0.45 g Sylgard® 184 Curing Agent and the solution was further mixed extensively with a vortex and poured onto a PTFE coated surface. The solution was then cured in darkness within a vacuum oven at 60 °C for 24 hr.

b. Activation under tension

Film strips were cut from a bulk sample in the general dimensions of 0.2 x 5.0 x 6.0 mm (thickness x width x length). Control films were placed in the oven among the loaded sample and the environment was brought to the test temperature at the fastest rate achievable (60°C/min). The film and oven temperature were permitted to equilibrate for 5 minutes. Individual films were then strained to 175% Figure 9) at a rate of 0.2 mm/s, held for 180 s, relaxed to initial strain at a rate of 0.4 mm/s, and promptly removed from the oven. Samples were then taken to a fluorescent microscope for analysis.

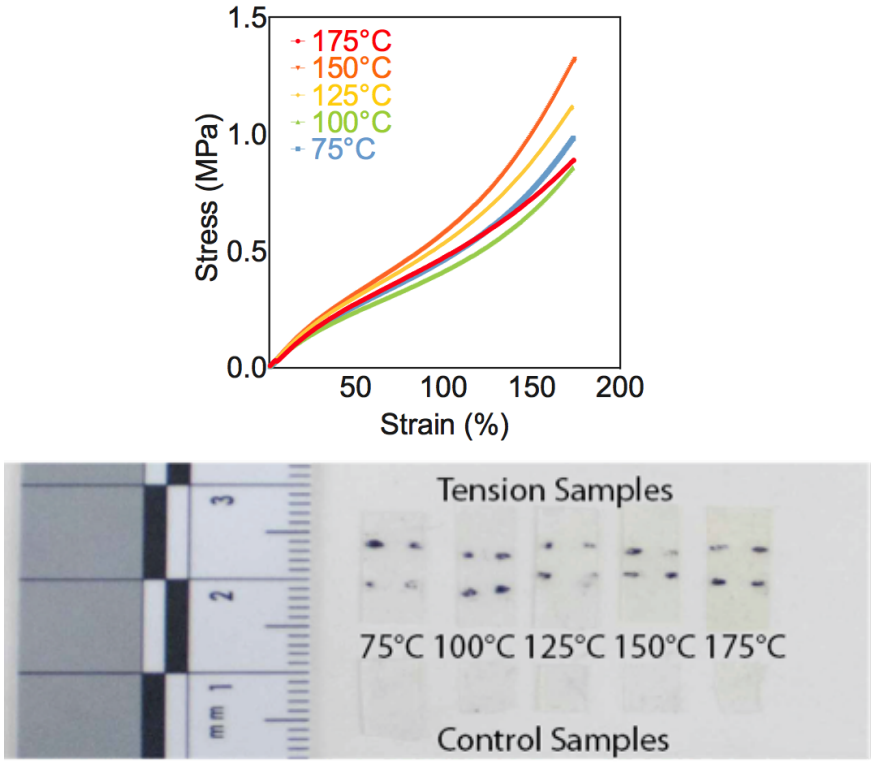

Figure 9. Loading curves of all films at the test temperatures and test samples (above) among control samples (below). Black permanent marker lines indicate the gauge region of the sample.

c. Image acquisition

All film samples were put onto a single PTFE printed microscope slide with segregated wells. Taking individual images of one film per microscope slide showed that the fluorescence emission of a neighboring film does not contribute to the observed intensity of a film in focus. Since all samples were too large for the entire ROI to be viewed with the largest objective available, multiple images were taken to be certain that the fluorescent intensity was homogeneous across the sample. Images were captured consecutively with a 5x objective and 50 ms exposure of a mercury lamp filtered through a DAPI cube (FS49: G365, FT395, BP445/50). The light was not attenuated.

d. Image processing

Acquired images were saved as 16-bit grayscale (0-1024) TIFFs and were processed with FIJI (ImageJ) software. From the array of images collected, the initial raw control images were chosen that

were representative of the entire sample, and tension images were chosen from the center of the gauge region of the tested film. (Figure 10A). To remove the raw camera noise, intensity from a region of an image off of the sample was subtracted from the whole of the image (Figure 10B). Because a thicker sample has a greater observed volume contributing to fluorescent intensity, a correction needed to be for intensity per volume of sample. Since fluorescent output is homogenous across the sample, samples can are normalized by dividing the 2-dimensional fluorescent intensity (i.e. integrated pixel intensities/pixel area in mm^2) of the entire image in by the depth of the sample to obtain a normalized fluorescent output in arbitrary units per unit volume (mm^3). Normalized images were then cropped (as indicated by the yellow squares) for the manuscript figure (Figure 10C). The graphs corresponding to the image intensities for the corrections are also shown (Figure 11).

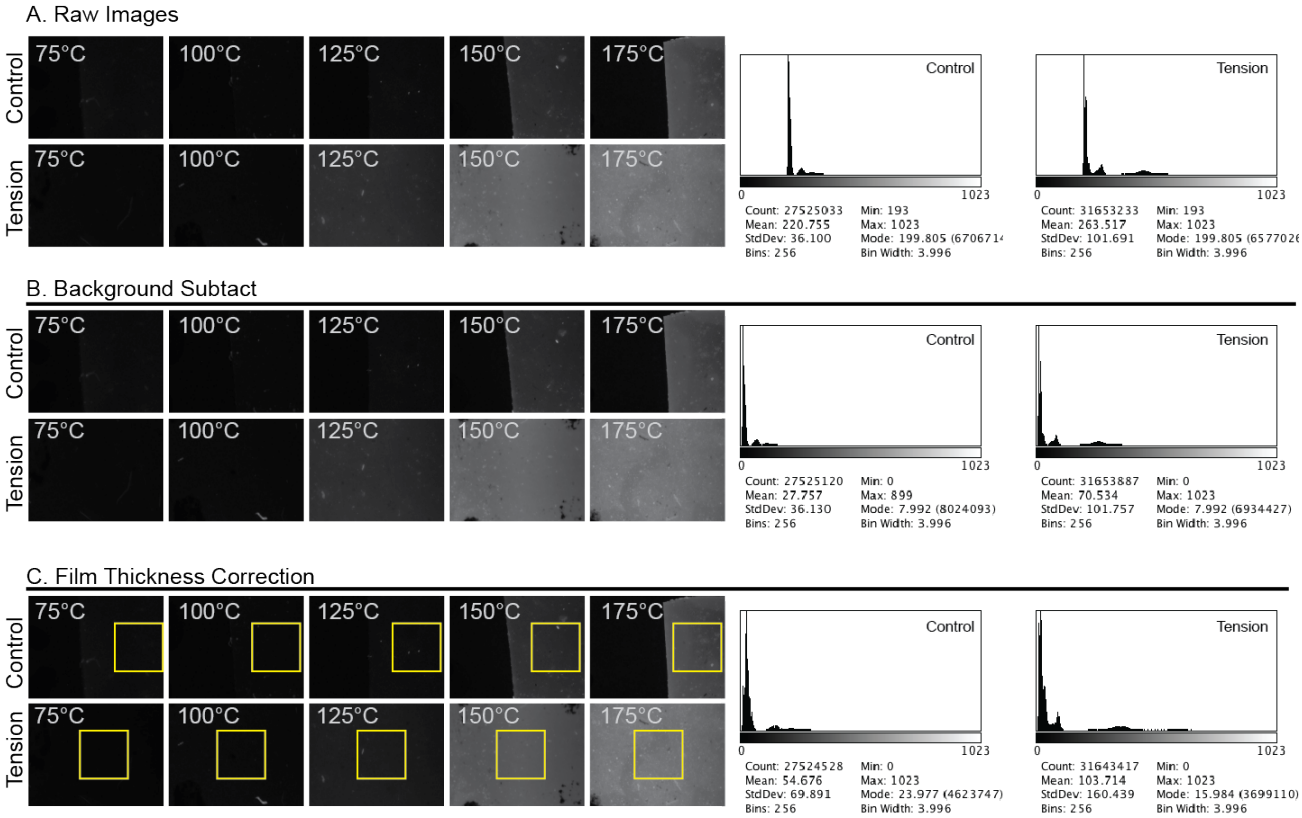

Figure 10. Raw images chosen from both tension and control for a given temperature (**A**). Removing the raw camera noise background corrects the images (**B**). Dividing images by a factor that corrects for the intensity densities results in the final images (**C**), with manuscript images taken in from the yellow insets.

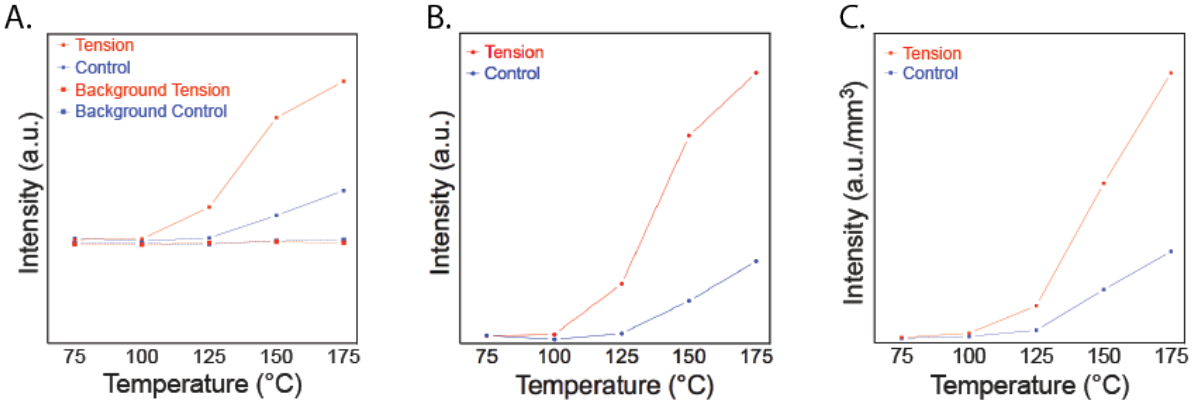

Figure 11. Graphical representations of the pixel intensities for the raw image (**A**), background corrected (**B**), and volume normalization (**C**) for the anthracene fluorescent intensity analysis.

e. Calibration Curve of Anthracene Fluorescent Intensity

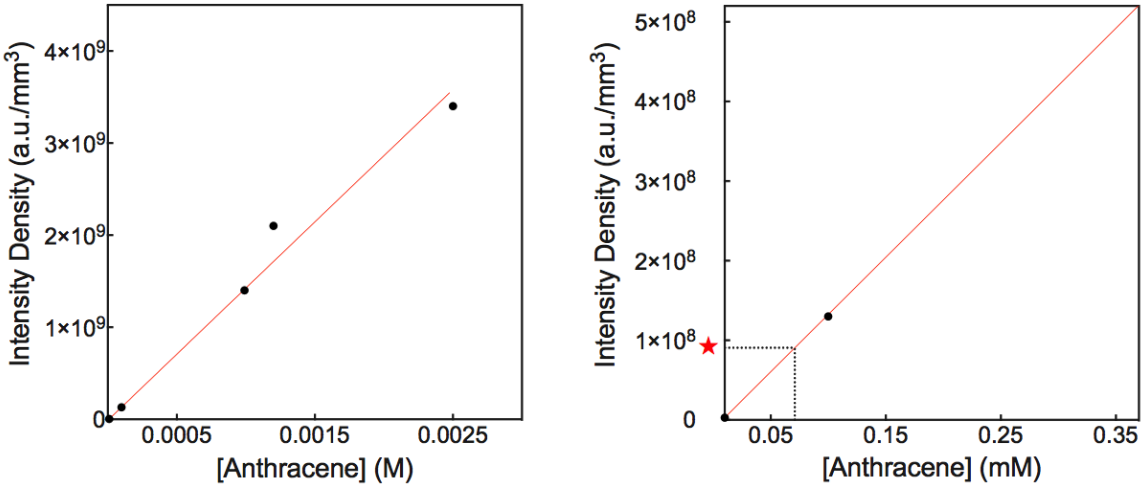

Figure 12. Calibration curve of fluorescent intensity from increasing anthracene concentration. Image on the left shows the linear region of fluorescent intensity vs. anthracene cross-linker concentration. The figure on the right is enhanced to show the region of lower concentration. The red star indicates the activation attributed to tension (1.2 MPa, 5 min) at 125 °C. This intensity corresponds to 1.1% mechanophore activation.

VIII. Active PDMS Colorswitch Experiment

a. Spectral data for color switch

Active PDMS samples were manually stretched by means of a modified loading frame (Figure 13, left) in oriented 45° relative to the incident excitation source and detector path. Since samples under uniaxial elongation both become thinner and display an increase in SP to MC conversion at higher strains, the absorption and emission intensities were normalized to emphasize relative peak maxima. Florescent emission spectra (532 nm excitation), for the stretched blue form, subsequently relaxed purple form, and 355 nm excitation spectra are shown (Figure 13, right).

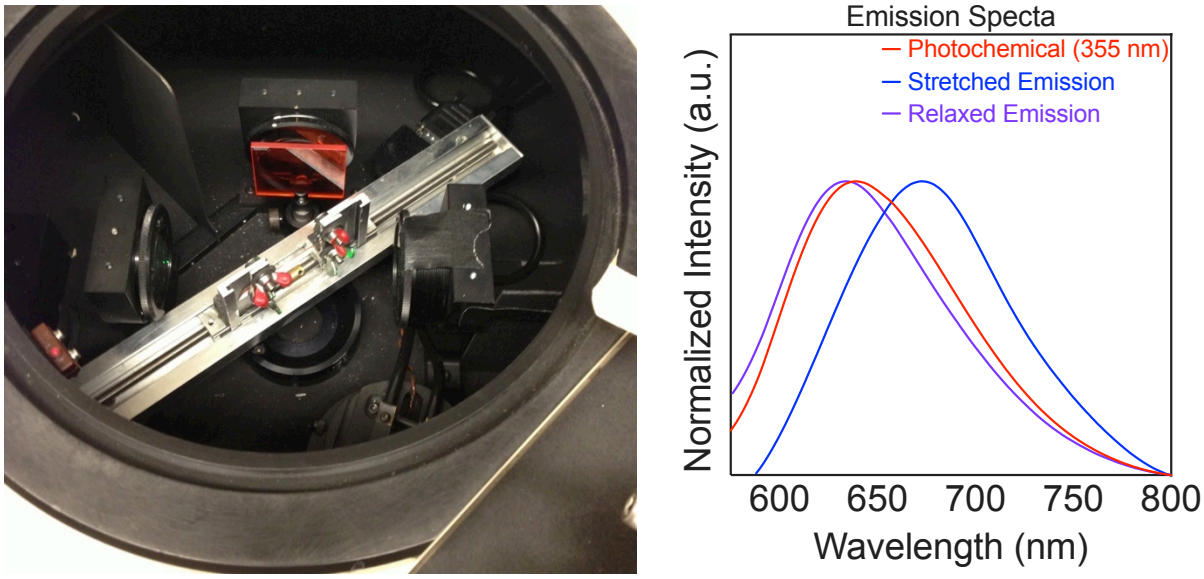

Figure 13. Stretched sample orientation within the spectrometer (Left) and emission plots from a 532 nm emission of spiropyran containing films.

Stretching a film reveals a blue color, which turns purple upon relaxation. The blue film's emission profile is red shifted from that of the purple (Figure 13B). Stretching the film a second time reveals the blue color once more, which can then be cycled back and forth between states as fast as the film can stretched and subsequently relaxed. Interestingly, the emission spectrum of the photochemically activated merocyanine is similar in both shape and peak-maximum as the relaxed form of the mechanically activated molecule (Figure 13B). Presumably, the electronic states leading to the emission are identical for the photochemically and mechanically are the same isomer.

We speculate that the blue/purple emission shift may be the result of an isomerization about the methine bridge of the merocyanine (Figure 14). Such a transition could arise from a force-biased shift in equilibrium from the thermally observed isomer (presumably TTC),[7,8] to a secondary metastable state of different photophysical properties. Noticeably the TTT and CTC isomers have a greater end-to-end distance from the chain attachment points, and would be the likely candidates a mechanical coupling leading to equilibrium bias. Ongoing work will investigate the structural basis of the color shift.

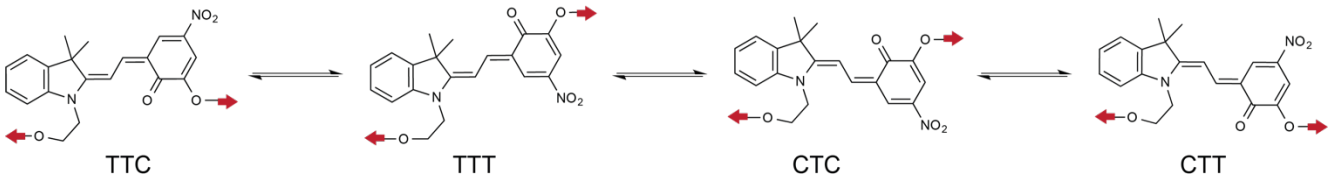

Figure 14. Various isomers of merocyanine about the methine bridge with attachment points shown for **5b**, isomer names are shown below the structure.

IX. Digital Image Processing

The digital images acquired here were often underexposed and orange in color as result of ambient room light. To standardize the images for comparison and clarity, each individual image was taken with a color neutral white card somewhere in the image. A white card possesses spectral neutrality and

uniformity under all sources of illumination and allows for all images to be calibrated and corrected to a known standard. Each image received the same treatment and no further processing was conducted.

a. Adobe® Photoshop® Lightroom 4: White balance procedure

Adobe Photoshop was used to import .CR2 raw file formats, which were then white balanced or exported as an unmodified cropped .JPG. An "as captured" raw image was warmer in color than the reported 8-bit RGB triplet values of (220, 224, 223). The yellow insets in Figure 15 show the triplet values of a neutral target area within the image. Selecting a neutral target area (Tools > White Balance Selector) informs the program of true color neutrality, which normalizes the three channels within the color neutral target (Figure 15B) and correspondingly adjusts the color characteristics of the entire image. Increasing the exposure (Basic > Exposure) brings the triplet values of the neutral target within the range of the reported values of the white balance card (Figure 15C). The value of gamma is left unchanged.

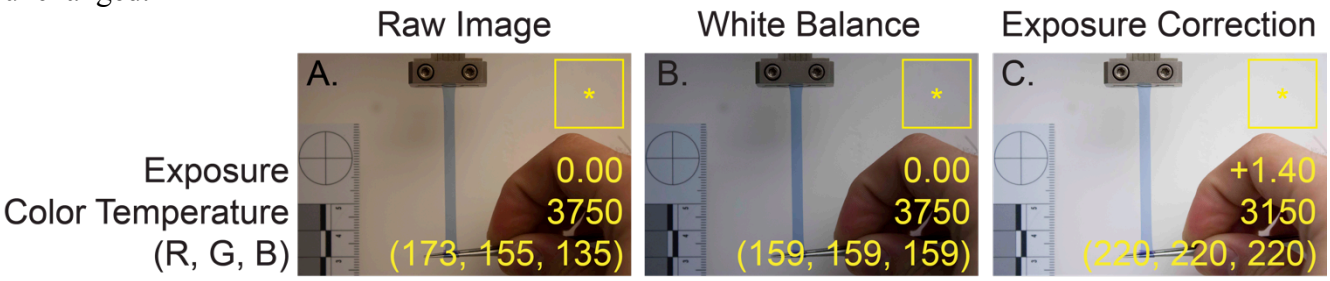

Figure 15. Digital image of activated film captured in RAW image format (**A**). RGB triplet values of white background are indicative of warmer room lighting and an underexposed image. White balance background target selected for color neutrality, RGB triplet values are normalized (**B**). Exposure is increased to make the image easier to see (**C**).

b. FIJI (ImageJ): White balance procedure

An equivalent operation to the one listed above is to use FIJI to perform a manual white balance correction. Color images are imported into FIJI as a .TIFF or other comparable format (Figure 16A). The RGB image is then split into individual RGB channels (Image > Color > Split Channels). For each channel, a neutral target of the image was selected (Figure 16B, white inset) and a histogram was obtained for each of the three channels (Figure 16C, Initial). The color neutral region in (Figure 16B) shows that the image has a warmer color temperature than natural, and the image is underexposed. The mean intensities of each channel were recorded from the histogram and whole-image intensities were multiplied by a factor that corrected the mean intensity of the neutral area to the reported 8-bit RGB triplet values of the white card (Process > Math > Multiply). Once the color stacks were white balanced they were restacked into a RGB composite (Image > Color > Merge Channels). From the histograms can be seen the original RGB composite histograms of the target region and the total image (Figure 16C, Initial). Post-correction the neutral target peak intensities have been normalized, which correspondingly corrected the whole image intensities (Figure 16C, Corrected).

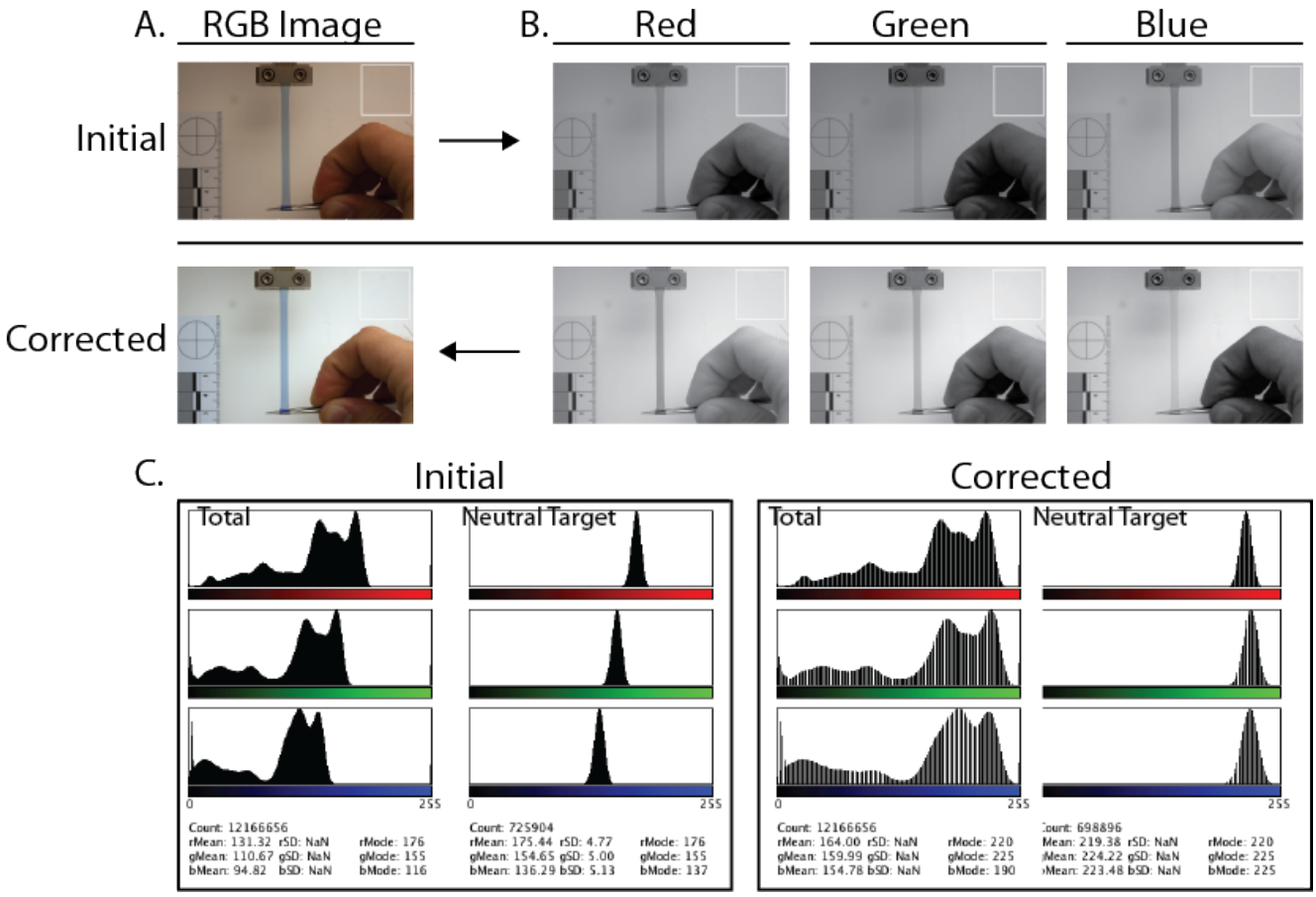

Figure 16. The initial RGB image (A) split into its individual R, G, B channels (B). Color correction to the individual stacks allows for the merged RGB composite to be white balanced to a spectrally neutral color target in image background. Initial and Corrected histograms show intensity normalization for the neutral target and its effect on the correction on the whole of the image (C).

X. References

(1) Davis, D. A.; Hamilton, A.; Yang, J.; Cremar, L. D.; Van Gough, D.; Potisek, S. L.; Ong, M. T.; Braun, P. V.; Martinez, T. J.; White, S. R.; Moore, J. S.; Sottos, N. R. *Nature* **2009**, *459*, 68.

(2) Um, M.-C.; Jang, J.; Kang, J.; Hong, J.-P.; Yoon, D. Y.; Lee, S. H.; Kim, J.-J.; Hong, J.-I. *J. Mater. Chem.* **2008**, *18*, 2234.

(3) Cammidge, A. N.; Goddard, V. H. M. *Liquid Crystals* **2008**, *35*, 1145.

(4) Mery, S.; Haristoy, D.; Nicoud, J.-F.; Guillon, D.; Monobe, H.; Shimizu, Y. *Journal of Materials Chemistry* **2003**, *13*, 1622.

(5) O'Bryan, G.; Wong, B. M.; McElhanon, J. R. *ACS Applied Materials & Interfaces* **2010**, *2*, 1594.

(6) Lee, C. K.; Davis, D. A.; White, S. R.; Moore, J. S.; Sottos, N. R.; Braun, P. V. *J. Am. Chem. Soc.* **2010**, *132*, 16107.

(7) Wohl, C. J.; Kuciauskas, D. *The Journal of Physical Chemistry B* **2005**, *109*, 22186.

(8) Minkin, V. I. *Chemical Reviews* **2004**, *104*, 2751.